Anomalous subdiffusion due to obstacles: A critical survey

Hugues Berry, Hugues Chaté

Anomalous subdiffusion due to obstacles : A critical survey

Hugues Berry[1]
EPI Combining,
INRIA, 69603 Villeurbanne, France

Hugues Chaté
Service de Physique de l'Etat Condensé,
CEA-Saclay, 91191 Gif-sur-Yvette, France

[1]Corresponding author. E-mail: hugues.berry@inria.fr; Address: EPI Combining, INRIA, La Doua Campus, Batiment CEI-1, BP 52132, 66 Blvd Niels Bohr Villeurbanne, 69603, France Tel.: 33(0)472-437-501, Fax: 33(0)472-438-313

Abstract

Passive molecular movements in cells are often claimed to exhibit "anomalous subdiffusion", where the mean-squared displacement (MSD) scales as a power law of time with exponent $\alpha < 1$. Diffusion hindrance by obstacles is often invoked to explain these observations. In many studies of hindered diffusion, the estimated values of α vary strongly. This led to the hypothesis that α depends on obstacle density. This is however at odds with the theoretical support for hindered diffusion among randomly located immobile obstacles, which predicts that true subdiffusion occurs only in the vicinity of the threshold for the percolation of obstacles, and that α takes a *unique*, universal value. Here, we present refined simulations of hindered diffusion with biologically realistic parameters and bring forth four main contributions. (*i*) We confirm that diffusion hindered by randomly located immobile obstacles does not exhibit variations of α and (*ii*) that the MSD in fact never scales like a power law of time. (*iii*) In contrast to diffusing obstacles, obstacles fluctuating around equilibrium positions preserve and even emphasize anomalous regimes. (*iv*) Hindered diffusion is not equivalent to anomalous diffusion due to random traps with heavy-tailed trap time distribution. These results shed new light on the existing literature about subdiffusion.

Key words: Anomalous Diffusion; Obstacle Hindered Diffusion; Macromolecular Crowding; Fluctuating Obstacles; Monte-Carlo Simulations; Percolation Theory

Introduction

A hallmark of Brownian motion is the linear relation between the average of the squared distance travelled by the molecule (mean squared displacement) and time: $\langle R^2(t) \rangle \propto t$. However, experimental measurements of molecular diffusion in living cells have consistently reported nonlinear relations in almost all cell compartments, either in procaryotes or eucaryotes. Most often, these nonlinear variations are claimed to be power laws ($\langle R^2(t) \rangle \propto t^\alpha$ with $\alpha \neq 1$), i.e. straight lines once represented on log-log plots.

Super-diffusive motion ($2 > \alpha > 1$) is relatively well understood, being usually due to active transport mediated by molecular motors on cytoskeleton elements (1), but subdiffusive transport ($\alpha < 1$) less so. Fundamentally, it is expected to arise when a hierarchy of slow processes hinders motion. Two classes of mechanisms yield such a situation: (a) a hierarchy of time scales exists due to transient capture of the diffusive molecule by traps (e.g. weak binding) with broadly-distributed trapping times (this is the so-called continuous-time random walks, or CTRW, model), or (b) it can result from the heterogeneous, irregular geometry of the space domain in which molecules move. In measurements in cells, it is usually unknown which one of these mechanisms is the cause of the observed anomalous behavior. This is a first source of ambiguity in the interpretation of experimental results.

Moreover, experimental works report strikingly different values of α. Continuously-varying exponents are consistent with the CTRW model, where the trap time distribution is power-law distributed $p(\tau) \propto \tau^{-\beta}$ with $1 < \beta < 2$: in this case, diffusion will be anomalous, with exponent $\alpha = \beta - 1$ (2, 3). However, it is not clear how such a distribution could arise in vivo. Moreover, several experiments have reported anomalous diffusion for cases where trapping can be excluded, i.e. for purely obstacle-hindered diffusion (macromolecular crowding) (4, 5). So, even though trapping can play a role *in vivo*, hindered diffusion has to be considered.

Theoretically, hindered diffusion, i.e. diffusion in the presence of volume-excluding immobile obstacles, corresponds to the movement of a random walker on a percolating cluster (the set left available by the obstacles). At an obstacle density at finite distance above the percolation threshold, the macroscopic percolating cluster is fractal only over short distances and appears uniform at larger scales (6). One expects then three diffusion regimes: Brownian ($\alpha = 1$) at short times (before the walker encounters obstacles), followed by a crossover to an anomalous regime with exponent $\alpha < 1$ at intermediate times and, finally, a second crossover back to normal diffusion ($\alpha = 1$) (2), which is the asymptotic regime. When the density of obstacles

changes, the two crossover times are predicted to vary: in particular the latter (from anomalous back to Brownian) is expected to diverge when the percolation threshold is approached (2). But a major prediction of the theory is that *the value of the exponent α is universal*, i.e. it does not depend on obstacle density, but essentially only on the (embedding) space dimension, taking respectively values $\alpha \approx 0.686$ and ≈ 0.526 in two and three dimensions (2).

Inside bacteria, experimental measurements of α for RNA particles in the cytoplasm gave estimates in the $[0.7 - 0.8]$ range (7). In the cytoplasm and nucleus of mammalian cells, diffusion of artificial markers yielded values ranging from $[0.5 - 0.6]$ (8), to $[0.6 - 0.8]$ (9). Such a large variability was also reported for GFP in the cytoplasm of mammalian cells (10). Reports of molecule diffusion on the plasma membrane of mammal cells are even less coherent. The diffusion of small fluorescent probes led to $\alpha \approx 0.74$ (i.e. not far from the value expected at the percolation threshold for $2d$) (11). But larger lipid-attached particles yielded a value *smaller* than this theoretical limit ($\alpha \approx 0.53$) (12), and studies using fluorescent-tagged receptors have reported huge variability across cells ($\alpha \in [0.2 - 1.0]$ (13, 14)). Finally, in the nucleus of mammal cells, the diffusion of Cajal bodies was found anomalous, with $\alpha \approx 0.67$ (15). But the diffusion of GFP or related proteins in nuclei also demonstrated large variability ($\alpha \in [0.65 - 0.9]$ (10)).

Such wildly varying estimates leave a confusing situation. To be true, most of the experimental curves in the above reports fail to display clearly identifiable power-law regimes, e.g. clean straight lines in log-log scales (12). In many cases, the anomalous regime is too short, i.e. lasts hardly more than a decade, to allow for the unambiguous identification of a true power-law regime and/or the number of points used to fit the data is too small (13, 15).

One would expect that the interpretation of experimental measurements *in vitro* should be easier. Diffusion in entangled meshes of semiflexible polymers can yield anomalous diffusion with exponent $\alpha = 3/4$ for particles larger than the mesh size (16). This regime has been observed during the diffusion of large particles in actin solutions (17) and in the cytosplasm of eucaryotic cells (see e.g. (18)). The mesh size of the actin network *in vivo* is however of the order of 1 μm (17) so that this anomalous regime is expected for molecular sizes at least several hundreds of nm, circa 2 orders of magnitude larger than most proteins. Diffusion of smaller molecules ($< 5 - 6$ nm) in polymer solutions is thus generally expected to be Brownian ($\alpha = 1$) but with a reduced apparent diffusion coefficient (19).

Nevertheless, several experimental studies (9, 20, 21) have reported anomalous diffusion of small artificial molecules or globular proteins in crowded

dextran solutions, claiming the observation of anomalous exponents with values decreasing from 1 to ≈ 0.70 when molecular crowding increases (9, 20). However, experimental error on the determination of α seems very large. Repeated measurements of α on the same experimental sample yield values that can vary from 0.7 to 0.9 across experiments (21). These results are further challenged by several contradictory experimental studies (19, 22, 23), that found only Brownian diffusion in similar or identical conditions. Taken together, these studies attest that even in *in vitro* and carefully controlled conditions, the processing of data is a step not free from various pitfalls, and the large variability of the reported results calls for caution in assessing their worth.

More intriguingly, even computer simulations of hindered diffusion have claimed crowding-dependent values of α (24, 25). This notion was first suggested more than 25 years ago in Argyrakis and Kopelman (26), where the diffusion of a random walker on a percolation cluster above the threshold was studied by computer simulations. However, the power law regime at intermediate times claimed in this paper is poorly convincing, especially because the simulations barely cover two time decades. Similarly, in published simulation results, the existence of a true power-law regime in the $(\log \left\langle R^2(t) \right\rangle \; vs \; \log t)$ curves is questionable (at least far from the threshold). First of all, the size of the spatial domain used in the simulations is very often small compared to the maximal average distance travelled by the molecules (24, 25, 27) so that finite size effects are to be expected. Moreover, simulation results often suffer from the same weaknesses as experimental ones, including small number of data points (9, 21) or short anomalous regimes with disputable evidence of a power law (28, 29).

Finally, it has been suggested that the anomalous regime observed may be crucially dependent on the dynamics (or lack of) of obstacles themselves. Indeed, when the obstacles are allowed to diffuse even at a much slower rate than the tracked molecule, the transient anomalous regime is predicted to disappear rapidly (27, 30). In fact, a recent theoretical study (31) predicts that when mobile obstacles and walkers have the same diffusion coefficient, the movement would be Brownian diffusion at long times and anomalous at short ones. But this predicted short-time anomalous diffusion regime is not a power law.

More recent works have moreover suggested an interesting possibility in the case where obstacle diffusion is small but non zero. In this case, one can envision the mobile obstacles as dynamic cages, transiently trapping the diffusing molecules. The lifetimes of these cages may be broadly distributed at high obstacle density, thus potentially leading to a situation similar to the

trapping-mediated anomalous diffusion (CTRW) evoked above (32). Such a situation would offer a plausible explanation for the reported variability of the anomalous exponent but remains to be tested by realistic simulations.

In the present work, our objective is to examine the issues raised above. Using refined simulations devoid of the shortcomings evoked above, we make four contributions :

- We confirm that hindered diffusion due to immobile obstacles does not give rise to anomalous regimes with crowding-dependent exponents. The anomalous exponent is unique, and obstacle density only modifies the crossover times between Brownian and anomalous regimes.

- For biologically realistic parameters, our simulations do not show evidence for even a transient power law behavior during the transient anomalous regime: the dynamics in this regime are completely dominated by crossovers.

- The effect of obstacle movements mainly depends on the type of movement considered. In agreement with previous works (27, 30), our simulations show that diffusing obstacles (undergoing Brownian motion) have a strong tendency to suppress anomalous regimes. But if the obstacles jitter around equilibrium average positions, the anomalous regime can persist at short times even with strong obstacle fluctuations.

- Finally, we show that, whatever the type of obstacle considered, one can measure a distribution of "effective trapping times" which slightly broadens with increasing obstacle density, but without exhibiting the heavy-tails characteristic of the CTRW model.

Methods

Simulations with immobile obstacles

We simulated the diffusion of tracer molecules using lattice-free domains with periodic boundary conditions (this reduces finite-size effects). Each run was initiated by positioning at random (with uniform probability) 2d (3d) obstacles in a 2d (3d) continuous domain of overall size $L_x \times L_y (\times L_z)$, until the volume fraction occupied by the obstacles equals the preset excluded volume fraction θ. A set of N_{w} non-interacting tracer molecules (walkers) was then positioned in the space domain at random locations but respecting

excluded volume w.r.t. obstacles: for each tracer molecule, a new position $\mathbf{x}_w$ is chosen at random (with uniform distribution) inside the simulation domain, until the tracer molecule does not overlap with any obstacle at $\mathbf{x}_w$.

At each time step, the simulation then proceeds by moving each tracer molecule (walker) independently of each other. We modeled diffusion using values for the time step δt and the displacement per time step δr that do not depend on the coefficient diffusion. Between t and $t + \delta t$, each molecule has a probability P_{move} to move to a randomly-chosen position located at distance δr from its position at t. The displacement probability is given by the diffusion coefficient D : $P_{\text{move}} = 2dD\delta t/\delta r^2$. The advantage of this algorithm is that, choosing a sufficiently small value for δr (namely $\delta r < 2r_{\text{w}} + 2r_{\text{obs}}$) ensures the excluded volume condition for all values of D and δt. In our simulations, typical values ranged from $P_{\text{move}} = 0.35$ to 0.95. Excluded volume is then modeled by adding the restriction that displacement attempts are rejected when the diffusing molecule, at the target site, overlaps with an obstacle.

The squared displacement $R^2(t)$ of each tracer molecule was monitored taking into account periodic boundary conditions. Unless otherwise indicated, $R^2(t)$ was averaged over $N_{\text{w}} = 10^4$ molecule trajectories per spatial obstacle configuration and 10 obstacle configurations.

Simulations with mobile obstacles

To model the diffusive movements of the obstacles, the position of each obstacle at time $t + \delta t$ was updated according to $\mathbf{r}_{\text{obs}}(t + \delta t) = \mathbf{r}_{\text{obs}}(t) + \mathbf{G}_d(\sigma_{\delta r})$ where $\mathbf{G}_d(\sigma_{\delta r})$ is a d-dimensional random vector of which each component is drawn independently from a normal distribution of mean 0 and standard deviation $\sigma_{\delta r}$. This setting results in a diffusive movement with diffusion coefficient $D_{\text{obs}} = \sigma_{\delta r}^2/(2\delta t)$.

Likewise, to simulate fluctuating obstacles, the position of each obstacle at time $t + \delta t$ was set according to $\mathbf{r}_{\text{obs}}(t + \delta t) = \mathbf{r}_{\text{obs}}(t_0) + \mathbf{G}_d(\sigma_{\delta r})$ where $\mathbf{r}_{\text{obs}}(t_0)$ is the equilibrium position of the obstacle . The quantity $\sigma_{\delta r}$ thus represents the amplitude of the obstacle fluctuations around their equilibrium position, i.e. their mobility. Note that in both cases obstacles do not experience excluded volume interactions with respect to each other and can thus interpenetrate.

Effective and approximate exponents

In many cases, a simple log-log plot of the MSD $\left\langle R^2(t)\right\rangle$ as a function of time is not accurate enough to validate or invalidate the existence of a power law regime. To improve the accuracy of the measurements, we computed the evolution with time of an effective exponent, $\alpha_{\text{eff}}(t)$, the local slope of the $\left\langle R^2(t)\right\rangle$ vs t relation in log-log scale: $\alpha_{\text{eff}}(t) = d\log\left\langle R^2(t)\right\rangle / d\log t$. The presence of a power-law regime then translates to an easily recognizable plateau in the $\alpha_{\text{eff}}(t)$ vs t curve.

Even though most of our results show that the $\left\langle R^2(t)\right\rangle$ vs t relation does not evidence a power law regime (ie a plateau in the $\alpha_{\text{eff}}(t)$ vs t curve), we define an *approximate* exponent, $\tilde{\alpha}$ as the minimal value of the $\alpha_{\text{eff}}(t)$ vs t curve, to allow for comparisons with published results.

Trapping time distribution

Mobile obstacles at high density are expected to form "dynamic cages" for the diffusing tracer molecule, that transiently form and disappear in time. Because of their stochastic and transient nature, they are difficult to define strictly. Here we consider that a tracer molecule is trapped by an obstacle whenever the tracer molecule remains within a distance r_{trap} (the trapping distance) of the obstacle. We then monitor the number of consecutive time steps spent by the tracer molecule within r_{trap} of every obstacle. These trapping times τ for each encounter of each obstacle and each molecule were then pooled to yield the trapping time distribution.

Results

Hindered diffusion by immobile obstacles

Our first goal here is to question the possibility that, for biologically relevant parameters, diffusion among immobile obstacles can give rise to anomalous scaling regimes with exponents that vary with the density of obstacles.

To avoid the issues encountered by previous simulation studies of hindered diffusion, we took care to monitor the mean-square displacement over large time scales (at least 6 decades) with a good sampling (> 700 data points per curve). The size of the spatial domain was set to $L_x = L_y = 5 \times 10^3 \times \delta r$ in 2d simulations and $L_x = L_y = L_z = 10^3 \times \delta r$ in 3d ones. Using these settings, the maximal mean travelled distance varied from 8.4 to 16.8 % of the length of the spatial domain in 2d, hence excluding finite size effects.

The typical values of the molecule and obstacle sizes and mobility were chosen so as to be representative of the size encountered in a typical bacterial cell. We considered an "average" protein in the cytoplasm of *E. coli* with radius $r_{\rm w} = 2.0$ nm and molecular weight 40 kDa (see e.g. TableS1 in McGuffee and Elcock (33)). The diffusion coefficient of the 28 kDa GFP in *E. coli* cytoplasm ranges from 2 to 10 μm^2/s while that of the 72 kDa GFP-MBP fusion protein is around 2.5 μm^2/s (34, 35). We accordingly set the diffusion coefficient of our 40 kDa "average" protein to within $D \in [4.0 - 8.0]$ μm^2/s. We considered large multimolecular obstacles, such as ribosomes, with radius $r_{\rm obs} = 5$ nm. In 3d simulations however, computational load demanded larger δr values and we had to increase $r_{\rm obs}$ to 10.0 nm.

Figure 1 shows the evolution with time of the MSD (Fig. 1A) as a log-log plot. Each curve in the figure corresponds to a different obstacle density. The top-most curve is for unobstructed diffusion, while obstacle density increases from top to bottom, until the lowest curve where 50% of space is occupied by obstacles (thus the excluded fraction $\theta = 0.50$).

Clearly, without obstruction, a single diffusion regime is found, with Brownian diffusion ($\alpha = 1$). When the excluded fraction is very high (e.g., $\theta = 0.50$, well above the percolation threshold located around $\theta = 0.44$, see below), the curves evidence saturation of the MSD, as space is partitioned into disconnected clusters of available sites which permanently trap the tracer molecules. For intermediate obstacle fractions ($\theta \lesssim 0.4$), three regimes can be distinguished, including two Brownian regimes: one at short times ($t \lesssim 10^{-3}$ ms) and another one at long times ($t \gtrsim 0.5$ ms). Note that, within the time scale of figure 1, the late Brownian regime is clearly reached only for the smallest obstacle densities. For larger obstacle densities, the curves are however clearly converging to it.

As is often the case, it is very delicate to tell from the ($\log \mathrm{MSD}\, vs\, \log t$) curves what happens in the intermediate-time regime. This is better seen from the time evolution of the local exponent $\alpha_{\rm eff}(t) = d \log \left\langle R^2(t) \right\rangle / d \log t$ (see Methods), which is shown in the bottom panel of Fig. 1A. Without obstacles, the local slope is 1.0 at all times. With increasing excluded fraction θ, $\alpha_{\rm eff}(t)$ first bends downward then converges back to 1.0 at long times. For the largest excluded fractions, the local slope shows a monotonous tendency to decay at long times, corresponding to the saturation seen in the MSD vs time curves (Fig. 1A, Top). The visual change in aspect of the local slope curves (upward vs downward curvature at long times) can be used to locate the percolation threshold (36). This allows us to estimate the critical excluded fraction $\theta_c = 0.441(2)$ (where the digit in parenthesis indicates incertitude). The long-time value of $\alpha_{\rm eff}(t)$ for $\theta = \theta_c$ yields an estimate for

the anomalous exponent α (at the threshold) : $\alpha = \alpha_{\rm eff}(t \to \infty, \theta \to \theta_c) = 0.68(4)$. This value is in good agreement with theoretical estimates from percolation theory ($\alpha \approx 0.686$ in 2d (2)).

A clear result from Fig. 1A is the absence of plateaus at crowding-dependent values for intermediate times and subthreshold obstacle densities. In fact, the only convincing plateau is obtained at the percolation threshold. This observation is confirmed by examination of the inset of Fig. 1A Bottom, that presents $\alpha_{\rm eff}(t)$ for refined simulations (increased total simulation time, improved statistics) close to the threshold. These data show that one has to be very close to the threshold, i.e. the value of θ must be less than 1% of its value at the threshold, and wait for a rather long time ($t \gtrsim 5$ ms), in order to obtain a convincing power law regime. When the excluded fraction $\theta < 0.99\theta_c$, the curves fail to evidence plateaus, but instead show a concave upward curvature. We thus conclude that Fig. 1A does not support the hypothesis of a power-law behavior with crowding-dependent exponents during the intermediate anomalous regime.

To test the robustness of this conclusion, we ran simulations in different conditions. Figure S1 in the Supplementary Information section shows simulations in 2d but with various sizes of the tracer molecule ($r_{\rm w} =$ 0.0 or 0.5 nm) and larger immobile obstacles ($r_{\rm obs} =$ 2.0 to 5.0 nm). The obtained results are very similar to that of Fig. 1A. Similar results were also obtained when the random walks evolve on a square lattice (not shown). We also ran three-dimensional simulations (Fig. 1B). Because of the prohibitive computational cost of such 3d simulations, we could not reach the same statistical quality as in the 2d simulations. In particular, the maximal mean travelled distance was closer to the length of the spatial domain. Despite these limitations, the conclusions are again similar to those brought about by the previous simulations. Our estimate for the anomalous exponent ($\alpha = 0.50(3)$) is in good agreement with the theory ($\alpha \approx 0.526$ in 3d (2)), and the estimated percolation threshold ($\theta_c = 0.87(1)$) also agrees with the value estimated in Ref. (36) (0.84). More importantly, these 3d simulations confirm the absence of local slope plateaus at intermediate times.

Taken together, these results show that hindered diffusion by immobile obstacles does not feature transient anomalous regimes with crowding-dependent exponents. Instead, in agreement with theoretical predictions, obstacle density only modifies the crossover times between Brownian and transient anomalous regimes. Furthermore, for biologically realistic sizes, the simulations do not even show trace of real power law behavior at all during the transient anomalous regime. Indeed, the dynamics in the intermediate regime is completely dominated by the crossovers from and back to

Brownian diffusion.

"Emulating" experimental results

The extensive simulations reported above indicate that the intermediate anomalous power law expected near the percolation threshold may actually not be observable, in opposition to several experimental reports. A first reason for this discrepancy could be that the conditions of experimental measurements are far from the ideal situation of the above simulations. To test this hypothesis, we ran simulations of hindered diffusion with "much lower quality" than our previous ones, so as to test conditions closer to reported experiments (section "Emulating experimental results" in the Supplementary Information). The results from these simulations (Figure S2) are indeed so imprecise that they can easily be misinterpreted in the sense of the existence of short pseudo-scaling laws.

Even though, strictly speaking, one cannot compute a proper anomalous exponent in the transient regime (because no power law regimes are found), our simulation results can be used to estimate an approximate exponent during the anomalous regime, in order to, for instance, compare our results with those of works discussing how so-called anomalous scaling exponents vary. To this aim, we fitted the ($\alpha_{\text{eff}}\, vs\, t$) curves (cf Fig. 1) by a nonlinear (log-normal) function to evaluate the minimal value of $\alpha_{\text{eff}}(t)$ on the simulated time interval (see Methods). This value was then used as a "rational" estimate of the approximate exponent, $\tilde{\alpha}$.

First of all, the measurements of $\tilde{\alpha}$ on our data, in Fig. 2, shows that when plotted against the relative distance to the threshold $\epsilon = 1-\theta/\theta_c$ (θ_c is the value of θ at the percolation threshold), the data for 2d simulations and various molecule sizes collapse on a single behavior. This collapse suggests a generic behavior for approximate exponent that would only depend on space dimension. Moreover, the 2d and 3d data could both be fitted by the same nonlinear function (the lines in Fig. 2):

$$\tilde{\alpha}\left(\epsilon\right) = \tilde{\alpha}_0 + \left(1-\tilde{\alpha}_0\right)\left(1+K\right)\frac{\epsilon}{K+\epsilon}. \tag{1}$$

For 2d data, we obtained $K^{(2d)} = 0.75 \pm 0.10$ and $\tilde{\alpha}_0^{(2d)} = 0.69 \pm 0.02$ and $K^{(3d)} = 0.23 \pm 0.03$ and $\tilde{\alpha}_0^{(3d)} = 0.49 \pm 0.01$ for the 3d case. Note that the value of $\tilde{\alpha}$ at the percolation threshold ($\epsilon = 0$) is given by the parameter $\tilde{\alpha}_0$ and is expected to correspond to the theoretical values predicted by percolation theory. In this perspective, our estimates for $\tilde{\alpha}_0$ are in very good agreement with theoretical values ($\alpha^{(2d)} \approx 0.686$, $\alpha^{(3d)} \approx 0.526$ (2)). Hence,

we think that Eq. 2 yields an accurate functional form for the dependence of the approximate anomalous diffusion coefficient on crowding density (see the Discussion section for comparison with experimental results).

Diffusion hindered by moving obstacles

The previous section showed that poor statistics and finite size effects encountered in typical experimental or numerical contexts may generate the appearance of pseudo-scaling laws with crowding-dependent exponents in the anomalous regime. This explains many of the disagreements between theory on the one hand and experimental and simulation reports on the other hand. However, several points remain unexplained, such as the reports of anomalous exponent values that are much *smaller* than the value expected at the percolation threshold (12) (see Introduction), although the latter is predicted to be the minimal accessible value. In this section, we examine the influence of obstacle mobility on the anomalous regime.

Figure 3A show simulations similar to those of Fig. 1A with obstacle density close to the percolation threshold (excluded volume fraction $\theta = 0.418$) but where obstacles move by Brownian diffusion. The reference curve in this figure is the red curve, that corresponds to $D_{\text{obs}} = 0$ i.e. immobile obstacles. The diffusion coefficient of the obstacles then progressively increases up to $D_{\text{obs}}/D = 568$, where D is the diffusion constant of the tracer molecules. The anomalous regime observed at long times with immobile obstacles (red curve) disappears as soon as $D_{\text{obs}}/D \gtrsim 1.0$ (green curve). Hence, these results show that anomalous diffusion is not expected to be observed at long times scales (around 0.1 ms) as soon as the obstacles diffuse, even with diffusion coefficient comparable to that of the tracer molecule. Note that this point was already suggested in Ref. (30), and partly in Ref. (37).

However, diffusive obstacle movements are not the only possible ones. Figure 3B shows simulations with obstacles that fluctuate around their equilibrium position. Note that in this figure, curves of the same color code for movements with identical mobility i.e. the same values of $\sigma^2_{\delta r}$ (see Methods). Comparing Fig. 3A & B, it is clear that, with fluctuating movements, anomalous diffusion is more robust. In fact, with fluctuating obstacles, diffusion remains fully anomalous up to mobilities $\sigma_{\delta r} \approx 1.0$ nm which corresponds to $D_{\text{obs}}/D = 5.7$ in the case of diffusive obstacles, i.e. a condition where the tracer movement is mostly Brownian. Thus, these results suggest that the transient diffusion regime could remain anomalous when obstacles fluctuate around equilibrium positions, even when these fluctuations are much larger than the mobility of the tracer molecule.

Another interesting property of anomalous diffusion with fluctuating obstacles is that when jitter amplitude is large enough, the fluctuations in effect remove the saturation of the MSD above the percolation threshold. Figure 4 shows MSD plots similar to those in Fig. 3B except that the density of fluctuating obstacles is varied (while the fluctuation intensity is kept constant at a rather high value of $\sigma_{\delta r} = 1.0$ nm). The top curve (the lavender one) corresponds to the same obstacle density as in Fig. 3B. Obstacle density is then progressively increased in the other curves of the figure, to values that would yield excluded fractions ranging from $\theta = 0.418$ to $\theta = 0.762$, if the obstacles were immobile. In other words, the density of obstacles used in Fig. 4 would be well above the percolation threshold with immobile obstacles ($\theta_c = 0.441$, see Fig. 1A). At first inspection, Fig. 4 shows that with very mobile fluctuating obstacles, the anomalous diffusion regime is preserved for all curves, i.e. even when the obstacle density is much larger than the percolation threshold. However, the first crossover time —from the initial normal diffusion to the anomalous regime— increases with the obstacle density.

Furthermore, a striking feature of the anomalous regimes obtained in suprathreshold conditions in Fig. 4 is that the obtained values of the anomalous exponent α (i.e. the value of the local exponent α_{eff} at the plateau) clearly decrease when the excluded volume fraction increases in the suprathreshold domain.The values of these anomalous exponents in the suprathreshold domain are even found significantly below the value expected at the percolation threshold. With $\theta = 0.709$ for instance (the bottom curve of Fig. 4), the value of α that would be deduced from the local slope for $t > 1$ ms is ≈ 0.40, which is much lower than theoretical value in 2d ($\simeq 0.69$). We thus propose that the presence of fluctuating obstacles in the suprathreshold domain may explain some of the experimental reports of crowding-dependent anomalous exponents α as well as the fact that some of these values may be smaller than their theoretical value at the percolation threshold.

Trapping time distributions

One way to interpret hindered diffusion is to consider that the obstacles form cages that temporarily trap the tracer molecules. When the obstacles are mobile, they can be considered to be forming dynamic cages whose lifetimes are expected to be broadly distributed at high obstacle densities (32). If this distribution is algebraic (and if the distribution exponent $\beta \in [1.0 - 2.0]$), one generically expects anomalous diffusion, through a mechanism that is essentially the same as that of the CTRW model (2, 3) (see Introduction). In particular, in this case, the anomalous diffusion exponent α would be

expected to vary continuously with β ($\alpha = \beta - 1$).

Because the traps formed by the moving obstacles are constantly reorganizing, it is difficult to define them. We opted for arguably the simplest definition. We considered that a walker is trapped by an obstacle as soon as the distance between them is less than some value r_{trap} (i.e. the distance between their centers is less than $r_{\text{trap}} + r_{\text{w}} + r_{\text{obs}}$). We thus measured the trapping time distribution of 2d tracer molecules in presence of $r_{\text{obs}} = 5$ nm obstacles that are either immobile (Fig. 5A), fluctuating (Fig. 5B) or diffusive (Fig. S3) . In each case, the first column presents conditions where the density of obstacles is low and diffusion remains Brownian throughout the simulation, whereas in the second column obstacle density and mobility were set so as to obtain a developed anomalous diffusion regime.

As expected, with small densities of immobile obstacles (Fig. 5A1) and for small values of the trapping distance r_{trap}, the trapping time distribution is exponentially distributed, reflecting the correlation time of Brownian motion. For larger r_{trap} values, the distribution tends to become bi-exponential. When immobile obstacles are the source of the anomalous diffusion regime (Fig. 5A2), the distributions become broader and exhibit a power law tail with exponent around -3.5. With fluctuating obstacles, trapping time distributions with low obstacle densities (thus yielding Brownian diffusion, Fig. 5B1) are very similar to those obtained with large obstacle densities (which yield anomalous diffusion, Fig. 5B2). In particular, in both case, the distributions display power-law tails with exponents around -3.8. Finally, in the case of diffusing obstacles, the distributions are qualitatively similar to the immobile case when diffusion is Brownian (Fig. S3A1), but with anomalous diffusion the power law-distributed long time tails observed above are much less obvious (Fig. S3A2).

Although we do not fully understand the various regimes observed, several interesting conclusions can already be drawn from these results. First of all, as expected, the distributions do broaden when obstacle density is large and diffusion anomalous. In certain cases, the distributions even show pronounced power-law tails. But we note that (*i*) in the case of mobile obstacles (either diffusing or fluctuating), the power law tails in the trapping time distributions are not specific to anomalous diffusion and (*ii*) the observed exponents β are found around $3.5-4.0$, whereas in the CTRW model, anomalous diffusion is expected only for $\beta \in [1.0, 2.0]$.

We thus conclude from these results that whatever the type of obstacle mobility, anomalous diffusion due to obstacles is not equivalent to a CTRW model, where anomalous diffusion would be explained by power-law distributed hopping times. Hence, this equivalence cannot be evoked

to explain the experimental observation of crowding-dependent anomalous diffusion exponents.

Discussion

The simulations reported here first of all confirm that hindered diffusion due to random immobile obstacles does not feature asymptotic anomalous scaling regimes where the exponent value would decay with obstacle density. The anomalous exponent is unique, only observable very near the percolation threshold, and obstacle density only modifies the crossover times between Brownian and anomalous regimes. Moreover, for biologically realistic parameters, the MSD dynamics is completely dominated by the crossovers from and back to Brownian diffusion.

One could first raise the issue of the realism of our simulation algorithms. We have used a simplified Monte-Carlo algorithm for molecule movement in a lattice-free space (see Methods). For a subset of the conditions illustrated in the paper, we have compared our results with simulations obtained using a more classical Brownian dynamics algorithm (where the distance travelled at each time step is a Gaussian random variable) or with simulations of diffusion on a lattice. We have not found differences in the ($\log \mathrm{MSD}\, vs\, \log t$) curves between these simulations and the ones illustrated above (not shown). More realistic diffusion models can be used, in particular using a real potential (e.g. Lennard-Jones) to simulate excluded volume or more realistic obstacle size distributions. Such an effort is accessible with modern day computing resources, albeit the total simulated real time is much smaller than in our paper (20 μs in. McGuffee and Elcock (33) versus $10-100$ ms in our case). Note however that, on their very short time scales, these detailed simulations are in general agreement with ours concerning the anomalous diffusion regimes (compare e.g. Figure 3B in McGuffee and Elcock (33) with the bottom panels of Fig. 1 in the present work). Hence, we think that our results are generic and robust to refinements of the model.

Yet, numerous experimental studies, in vitro (5, 9, 20, 21) as well as in vivo (7–13, 15), have consistently reported anomalous diffusion regimes with variable values of the exponent α. A first explanation could reside in experimental limitations. Indeed, three major methods have been used to measure molecular diffusion in these conditions : single-particle tracking (SPT), fluorescence recovery after photobleaching (FRAP) and fluorescence correlation spectroscopy (FCS). Experimental errors in the determination of particle positions in SPT experiments has been shown to lead to spurious

(subdiffusive) power law regimes at short times (38). FRAP studies usually are limited in measurement time, which impedes the analysis of the long-tail phenomena expected in anomalous diffusion (19). FCS is also problematic as it rests on the time-correlation function of the fluorescent light emitted from the proteins, whose functional form is known for Brownian diffusion. The analytical formulation of the FCS correlation function is not available for anomalous diffusion, so that an adhoc function is usually employed, that lacks real theoretical support (8) (albeit recent advances could improve this caveat (5)). Hence, even in in vitro and carefully controlled conditions, the experimental determination of some α value is very delicate. Moreover, independently from the measurement methods, the quantification of α in living cells could be influenced by intrinsic limitations due to the characteristics of the cell itself. In particular, our simulations (Fig. S2) show that the finite size of the cells and/or the low statistics inherent to in vivo measurements, could by themselves give rise to spurious power law-like regimes, that would naturally be interpreted as crowding-dependent anomalous exponents.

Another possible explanation could reside in the mobility of the obstacles. Indeed, our simulations confirm the conclusion of previous studies that the long-time anomalous regime typical of immobile obstacle disappears very rapidly as soon as the obstacles are mobile. However, our finding that diffusion amidst fluctuating obstacles gives rise to extended anomalous regimes has interesting implications. First, the case of fluctuating obstacles seems rather relevant in the context of biological cells. Fluctuating obstacles could arise when they self-organize into noncrystalline but organized supramolecular structures such as gel-like networks. This includes of course intracellular networks such as the actin or spectrin ones. For instance, a recent study measured the amplitudes of individual (i.e. not population averaged) MSDs of tracer particles within cytoplasms of eucaryotic cells (39) and showed they need circa 10s to decorelate, thus suggesting intracellular rearrangements of the cytoskeleton or internal macromolecular complexes. This is thus an indirect support for the existence of a long range spatial self-ordering that could lead to fluctuating obstacle structures. But fluctuating obstacles may be even more generically encountered. For instance, light-harvesting complexes of photosynthetic membranes are large-size obstacles that occupy between 70 and 90% of the membrane area (30). Recent experimental observations revealed that their mobility in the membrane indeed consists of fluctuations around an equilibrium position, with fluctuation amplitudes that depend on the considered region in the membrane (40).

Interestingly, our results with fluctuating obstacles could also explain some of the experimental reports obtained in vitro for tracers diffusing in

concentrated mobile crowders. Horton et al. (5) for instance, studies 2d diffusion on artificial lipid bilayer membranes with avidin as both the crowder and the tracer. This study shows that even at small densities, avidin self-organizes into a spatially heterogeneous (possibly gel-like) structure, that persists (i.e. does not mix) for several tens of minutes. This type of spatial heterogeneity is typically expected to yield fluctuating obstacles. In agreement with our simulation results for fluctuating obstacles (Fig. 3B), the authors find clear evidence for transient anomalous diffusion. Their measurements are also in striking agreement with our simulation results. For instance, the evolution with obstacle density of their estimates for the anomalous exponent (their Figure 5) has a shape very similar to our figure of the evolution of the approximate exponent $\tilde{\alpha}$ with the excluded fraction, Fig. 2 (which is not the case for the functional dependence proposed with mobile soluble crowders (20)). Moreover, the estimation of the minimal value of the anomalous exponent in Horton et al. (5) (0.68) is also in very good agreement with our estimates in 2d (0.69). We consider that this very good correspondence between these experimental results and our simulations is a confirmation of the robustness of our prediction for fluctuating obstacles.

Finally, we also presented evidence that whatever the type of mobility (or immobility), hindered diffusion due to obstacles is not equivalent to the CTRW model for trapping-based anomalous diffusion. The distribution of trapping-times due to the presence of obstacles broadens when the density of obstacles is large enough to yield anomalous diffusion, but it does not become a power-law with exponent in $[1.0 - 2.0]$, which is a mandatory prerequisite to yield anomalous diffusion in the CTRW model. Alternatively, the experimental observations of anomalous diffusion with crowding-dependent exponents could be explained by a real CTRW model, that is, it could arise if the movements of the tracer due to pure Brownian diffusion (i.e. in an homogeneous space) were combined to weak reversible binding events to other molecular species. However, in this case again, the binding times must be power-law distributed with an exponent restricted to a narrow range. It is not clear how such a process could be obtained in a living cell.

Hence, the major conclusion from this work is that, if one considers hindered diffusion due to obstacles as being the main source of anomalous diffusion within cells, the experimental observations of crowding-dependent anomalous diffusion are either spurious experimental results if obstacles are immobile or can be explained if the obstacles are present in high density and fluctuating around equilibrium positions within self-organized spatial structures.

Acknowledgments

The authors thank Fernando Peruani (MPI, Dresden, Germany) and Kazumasa Takeuchi (Univ. Tokyo, Japan and CEA, Saclay, France) for critical reading and useful suggestions about this article. We moreover acknowledge the support of the computing centre of CNRS IN2P3 in Lyon (http://cc.in2p3.fr), where the simulations were performed. This research was funded by the French National Institute for Research in Computer Science and Control (INRIA, grant "Action d'Envergure ColAge") and the French National Agency for Research (ANR, grant "PAGDEG ANR-09-PIRI-0030").

References

1. Kulic, I. M., A. E. X. Brown, H. Kim, C. Kural, B. Blehm, P. R. Selvin, P. C. Nelson, and V. I. Gelfand, 2008. The role of microtubule movement in bidirectional organelle transport. *Proc. Natl. Acad. Sci. USA* 105:10011–10016.

2. Bouchaud, J.-P., and A. Georges, 1990. Anomalous diffusion in disordered media: Statistical mechanisms, models and physical applications. *Physics Reports* 195:127 – 293.

3. Metzler, R., and J. Klafter, 2000. The random walk's guide to anomalous diffusion: a fractional dynamics approach. *Physics Reports* 339:1 – 77.

4. Ratto, T. V., and M. L. Longo, 2002. Anomalous Subdiffusion in Heterogeneous Lipid Bilayers. *Langmuir* 19:1788–1793.

5. Horton, M. R., F. Hofling, J. O. Radler, and T. Franosch, 2010. Development of anomalous diffusion among crowding proteins. *Soft Matter* 6:2648–2656.

6. Havlin, S., and D. Ben-Havraham, 1987. Diffusion in disordered media. *Adv. Phys.* 36, 695-798.

7. Golding, I., and E. Cox, 2006. Physical nature of bacterial cytoplasm. *Phys. Rev. Lett.* 96:098102.

8. Guigas, G., C. Kalla, and M. Weiss, 2007. The degree of macromolecular crowding in the cytoplasm and nucleoplasm of mammalian cells is conserved. *FEBS Lett.* 581:5094–5098.

9. Weiss, M., M. Elsner, F. Kartberg, and T. Nilsson, 2004. Anomalous subdiffusion is a measure for cytoplasmic crowding in living cells. *Biophys. J.* 87:3518–3524.

10. Wachsmuth, M., W. Waldeck, and L. J., 2000. Anomalous diffusion of fluorescent probes inseide living cell nuclei investigated by spatially-resolved fluorescence correlation spectroscopy. *J. Mol. Biol.* 298, 677-689.

11. Schwille, P., J. Korlach, and W. Webb, 1999. Fluorescence correlation spectroscopy with single-molecule sensitivity on cell and model membranes. *Cytometry* 36, 176-182.

12. Murase, K., T. Fujiwara, Y. Umemura, K. Suzuki, R. Iino, H. Yamashita, M. Saito, H. Murakoshi, K. Ritchie, and A. Kusumi, 2004. Ultrafine membrane compartments for molecular diffusion as revealed by single molecule techniques. *Biophys J* 86:4075–4093.

13. Smith, P. R., I. E. Morrison, K. M. Wilson, N. Fernndez, and R. J. Cherry, 1999. Anomalous diffusion of major histocompatibility complex class I molecules on HeLa cells determined by single particle tracking. *Biophys J* 76:3331–3344.

14. Vrljic, M., S. Y. Nishimura, S. Brasselet, W. E. Moerner, and H. M. McConnell, 2002. Translational diffusion of individual class II MHC membrane proteins in cells. *Biophys. J.* 83:2681–2692.

15. Platani, M., I. Goldberg, A. I. Lamond, and J. R. Swedlow, 2002. Cajal body dynamics and association with chromatin are ATP-dependent. *Nat Cell Biol* 4:502–508.

16. Gittes, F., and F. C. MacKintosh, 1998. Dynamic shear modulus of a semiflexible polymer network. *Phys. Rev. E* 58:R1241–R1244.

17. Amblard, Maggs, Yurke, Pargellis, and Leibler, 1996. Subdiffusion and Anomalous Local Viscoelasticity in Actin Networks. *Phys Rev Lett* 77:4470–4473.

18. Caspi, A., R. Granek, and M. Elbaum, 2002. Diffusion and directed motion in cellular transport. *Phys. Rev. E* 66, 011916.

19. Dix, J. A., and A. S. Verkman, 2008. Crowding effects on diffusion in solutions and cells. *Annu Rev Biophys* 37:247–263.

20. Banks, D., and C. Fradin, 2005. Anomalous diffusion of proteins due to molecular crowding. *Biophys. J.* 89:2960–2971.

21. Szymanski, J., and M. Weiss, 2009. Elucidating the origin of anomalous diffusion in crowded fluids. *Phys. Rev. Lett.* 103:038102.

22. Dauty, E., and A. S. Verkman, 2004. Molecular crowding reduces to a similar extent the diffusion of small solutes and macromolecules: measurement by fluorescence correlation spectroscopy. *J Mol Recognit* 17:441–447.

23. Sanabria, H., Y. Kubota, and M. Waxham, 2007. Multiple diffusion mechanisms due to nanostructuring in crowded environments. *Biophys. J.* 92:313–322.

24. Berry, H., 2002. Monte carlo simulations of enzyme reactions in two dimensions: fractal kinetics and spatial segregation. *Biophys J* 83:1891–1901.

25. Nicolau, D., J. Hancock, and K. Burrage, 2007. Sources of anomalous diffusion on cell membranes: a Monte Carlo study. *Biophys. J.* 92:1975–1987.

26. Argyrakis, P., and R. Kopelman, 1984. Fractal to euclidean crossover and scaling for random walkers on percolation clusters. *J. Chem. Phys.* 81:1015–1018.

27. Saxton, M. J., 1994. Anomalous diffusion due to obstacles: a Monte Carlo study. *Biophys. J.* 66:394–401.

28. Niehaus, A., D. Vlachos, J. Edwards, P. Plechac, and R. Tribe, 2008. Microscopic simulation of membrane molecule diffusion on corralled membrane surfaces. *Biophys. J.* 94:1551–1564.

29. Wedemeier, A., H. Merlitz, C.-X. Wu, and J. Langowski, 2007. Modeling diffusional transport in the interphase cell nucleus. *J. Chem. Phys.* 127:045102.

30. Tremmel, I. G., H. Kirchhoff, E. Weis, and G. D. Farquhar, 2003. Dependence of plastoquinol diffusion on the shape, size, and density of integral thylakoid proteins. *Biochim Biophys Acta* 1607:97–109.

31. Fanelli, D., and A. J. McKane, 2010. Diffusion in a crowded environment. *Phys. Rev. E* 82:021113.

32. Condamin, S., V. Tejedor, R. Voituriez, O. Bénichou, and J. Klafter, 2008. Probing microscopic origins of confined subdiffusion by first-passage observables. *Proc Natl Acad Sci U S A* 105:5675–5680.

33. McGuffee, S. R., and A. H. Elcock, 2010. Diffusion, Crowding & Protein Stability in a Dynamic Molecular Model of the Bacterial Cytoplasm. *PLoS Comput Biol* 6:e1000694.

34. Elowitz, M. B., M. G. Surette, P. E. Wolf, J. B. Stock, and S. Leibler, 1999. Protein mobility in the cytoplasm of Escherichia coli. *J. Bacteriol.* 181:197–203.

35. Konopka, M. C., I. A. Shkel, S. Cayley, M. T. Record, and J. C. Weisshaar, 2006. Crowding and Confinement Effects on Protein Diffusion In Vivo. *J. Bacteriol.* 188:6115–6123.

36. Höfling, F., T. Franosch, and E. Frey, 2006. Localization Transition of the 3D Lorentz Model and Continuum Percolation. *Physical Review Letters* 96:165901.

37. Saxton, M., 1990. Lateral diffusion in a mixture of mobile and immobile particles: A Monte Carlo study. *Biophys. J.* 58:1303–1306.

38. Martin, D. S., M. B. Forstner, and J. A. Ks, 2002. Apparent subdiffusion inherent to single particle tracking. *Biophys J* 83:2109–2117.

39. Duits, M. H. G., Y. Li, S. A. Vanapalli, and F. Mugele, 2009. Mapping of spatiotemporal heterogeneous particle dynamics in living cells. *Phys Rev E Stat Nonlin Soft Matter Phys* 79:051910.

40. Scheuring, S., and J. N. Sturgis, 2006. Dynamics and diffusion in photosynthetic membranes from rhodospirillum photometricum. *Biophys J* 91:3707–3717.

Figure Legends

Figure 1.

Evolution of the mean-squared displacement (*Top Row*) and corresponding effective exponent $\alpha_{\rm eff}$ (*Bottom Row*) during hindered diffusion by immobile obstacles in two (A) or three (B) dimensions. (**A**) 2d diffusion with excluded volume fraction $\theta = 0$, 0.06, 0.12, 0.17, 0.22, 0.27, 0.31, 0.36, 0.40, 0.41, 0.42, 0.43, 0.45, 0.47 and 0.50 (from top to bottom). $r_{\rm w} = 2.0$ nm, $r_{\rm obs} = 5.0$ nm, $D = 4.4\ \mu{\rm m}^2/{\rm s}$. *Inset* : Refined simulations with averages over 400 obstacle configurations and $\theta = 0.4345$, 0.4365, 0.4380, 0.4400, 0.4405, 0.4410, 0.4415, 0.4430, 0.4450 (from top to bottom). Resulting estimates are $\theta_c = 0.441(2)$ and $\alpha = 0.68(4)$. (**B**) 3D diffusion with $\theta = 0$, 0.567, 0.766, 0.843, 0.867, 0.874 and 0.876 (from top to bottom). $r_{\rm w} = 2.0$ nm, $r_{\rm obs} = 10.0$ nm, $D = 7.7\ \mu{\rm m}^2/{\rm s}$. These data yield $\theta_c = 0.87(1)$ and $\alpha = 0.50(3)$. All data are averages over 10^4 walkers per obstacle configurations and 10 obstacle configurations. Other parameters : $\delta t = 20$ ns, $\delta r = 1.0$ nm and $L_x = L_y = 5.0\ \mu$m (2d) or $L_x = L_y = L_z = 1.0\ \mu$m (3d).

Figure 2.

Variations of the approximate anomalous exponent $\tilde{\alpha}$ as a function of excluded volume fraction θ. Space dimension, radius of the random walker and of the obstacles were $\{d, r_{\rm w}, r_{\rm obs}\} = \{2, 0.0, 5.0\}$ (triangles), $\{2, 0.5, 2.0\}$ (times signs), $\{2, 2.0, 5.0\}$ (plus signs) or $\{3, 2.0, 10.0\}$ (circles). The lines show nonlinear fits (see text for the function used and the parameter estimates) : the full (blue) line is a fit of all data points in 2d series as a whole, while the dashed (green) one is a fit of the 3d series. The values of $\theta_{\rm c}$ were estimated from $\alpha_{\rm eff} = f(t)$ curves (Fig. 1 and S1).

Figure 3.

2D-diffusion hindered by mobile obstacles with various mobility. (**A**) Obstacles with diffusive motion. The obstacle-to-walker ratio of diffusion coefficients, $D_{\rm obs}/D = 0.0, 5.7 \times 10^{-4}, 1.42, 5.68, 35.5, 142, 320$ and 568 (from bottom to top in the bottom panel). (**B**) Obstacles with fluctuating motion. The amplitude of the obstacle fluctuations are chosen identical to

that yielding diffusive motions in (A), i.e (from bottom to top in the bottom panel) $\sigma_{\delta r} = 0.0, 0.01, 0.50, 1.0, 2.5, 5.0, 7.5$ and 10.0 nm. In both cases, the number of obstacles corresponded to $\theta = 0.418$ with immobile obstacles (i.e. close to the percolation threshold). Averages taken over 10^3 walkers per obstacle configurations and 10 different obstacle configurations. Other parameters : $D = 4.4\ \mu\text{m}^2/\text{s}$, $\delta t = 20$ ns and $L_x = L_y = 5.0\ \mu$m.

Figure 4.

Anomalous diffusion with fluctuating obstacles beyond the percolation threshold. Excluded volume fraction $\theta = 0.418$, 0.586, 0.646, 0.709 and 0.762 from top to bottom, i.e. well above the percolation threshold with immobile obstacles (compare with figure 1A). Obstacle mobility was $\sigma_{\delta r} = 1.0$ nm. All other parameters were the same as figure 3B.

Figure 5.

Trapping times distributions for hindered diffusion by immobile (A) or fluctuating (B) obstacles. In panels (A1, B1), obstacle density is low enough ($\theta = 0.031$) so that diffusion is Brownian throughout the simulation (see figure 1A) whereas in panels (A2, B2), obstacle density is close to the threshold ($\theta = 0.441$) and diffusion is strongly anomalous. For mobile obstacles, mobility was chosen small enough to preserve anomalous behavior, i.e. $\sigma_{\delta r} = 1.0$ nm for fluctuating obstacles (B) (see figure 3). In each panel, the trapping distance $r_{\text{trap}} = 0.5$, 1.0, 2.50 and 5.0 nm (from top to bottom), respectively. Each curve is averaged over 10^3 walkers per obstacle configurations and 100 obstacle configurations. The dashed lines locate power laws with exponent -3.5 (A2) or -3.8 (B1-2). Other parameters: $r_{\text{w}} = 2.0$ nm, $r_{\text{obs}} = 5.0$ nm, $D_{\text{w}} = 4.4\ \mu\text{m}^2/\text{s}$, $\delta t = 20$ ns, $L_x = L_y = 5.0\ \mu$m.

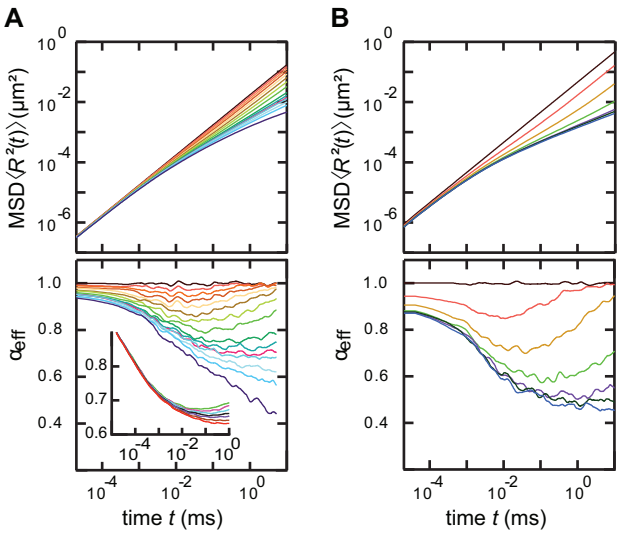

Figure 1:

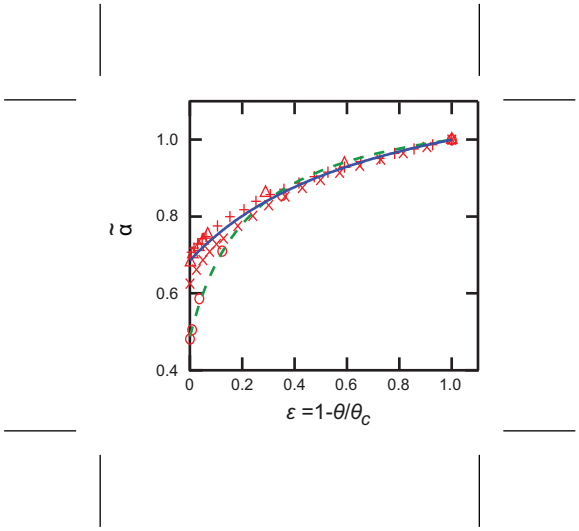

Figure 2:

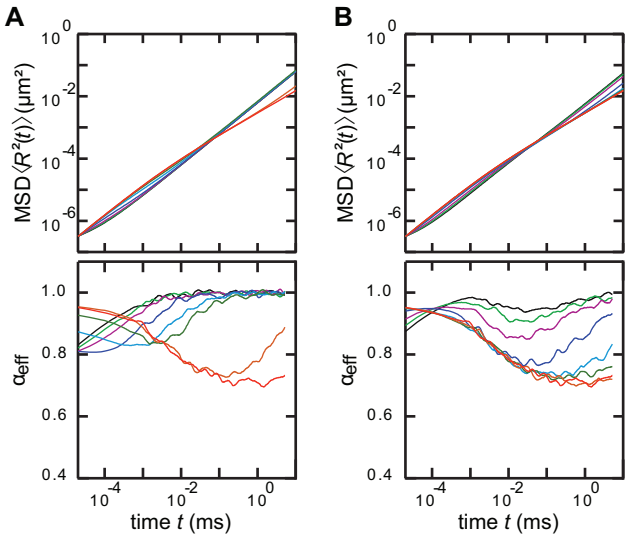
A
B
MSD ⟨R²(t)⟩ (μm²)
10^0
10^-2
10^-4
10^-6
α_eff
1.0
0.8
0.6
0.4
10^-4
10^-2
10^0
time t (ms)

Figure 3:

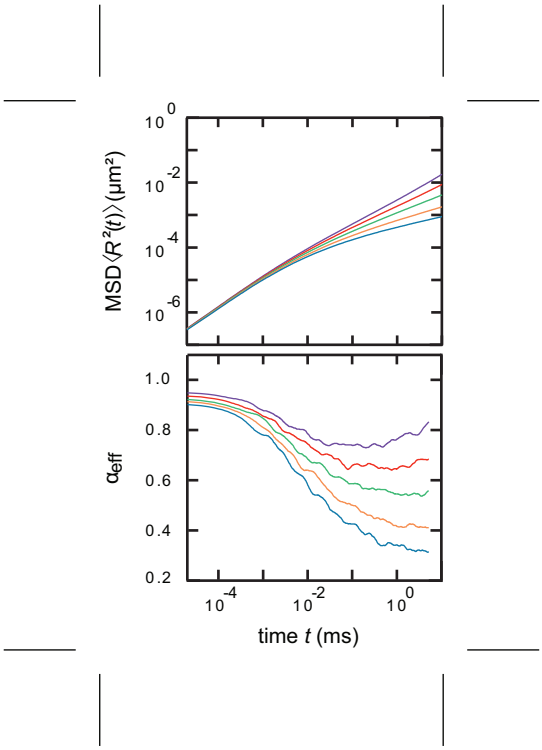
MSD ⟨R²(t)⟩ (μm²)
10^0
10^-2
10^-4
10^-6
α_eff
1.0
0.8
0.6
0.4
0.2
10^-4
10^-2
10^0
time t (ms)

Figure 4:

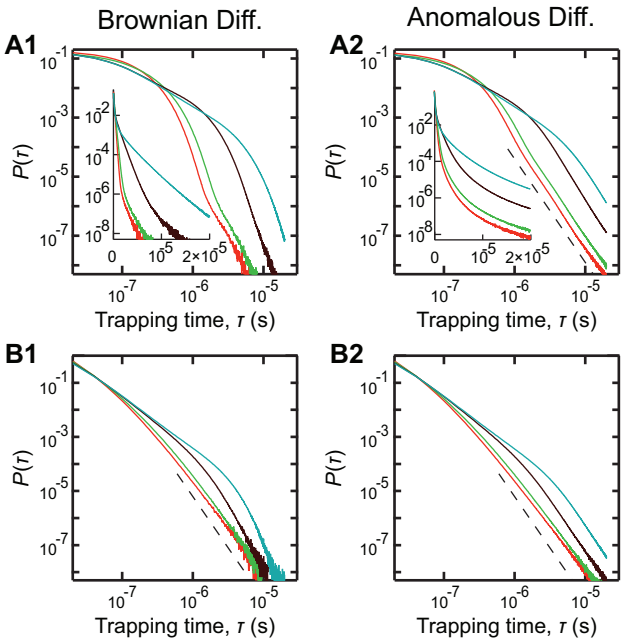

Figure 5:

Supplementary Informations

Emulating experimental results

The extensive simulations reported above thus confirm the theoretical viewpoint of a *unique anomalous exponent* α whatever the intensity of molecular crowding. They also indicate that the expected intermediate anomalous power law may actually not be observable because it is often masked by the crossovers. Now, experimental data have consistently reported anomalous power laws at intermediate times with variable exponents (see Introduction). How to explain such a discrepancy? A first possibility would be that the conditions of experimental measurements are far from the ideal situation of the above simulations. To test this hypothesis, we ran simulations of hindered diffusion with "much lower quality" than our previous ones, so as to test conditions closer to reported experiments. In particular, we took into account the fact that the spatial domain in real experiments is usually limited by the size of the cell or the subcellular compartment in which the molecule diffusion is restricted. The quality of the statistics of the data in the experiments is also expected to be lower and usually, the sampling of the data points in time is much lower.

Figure S2 shows three-dimensional simulations in a space domain whose volume is one hundredth that of the one used in Fig. 1B above. In fact, the maximal mean travelled distance in Fig. S2 is more than 5-fold the length of the space domain (we used periodic boundary conditions). We moreover averaged the data over a number of molecule per run that is ten times lower and a number of run that is only one third that of Fig. 1B. Finally, sampling frequency of the simulation to plot the results was also divided by ≈ 50, yielding only 12 data points per curve. This figure illustrates the fact that the conjugation of poor statistics with finite size effects leads to the appearance of regimes in the local exponent curves that look very close to horizontal (Fig. S2, Bottom). Importantly, the value of the local exponent (i.e. the value at the plateau) during these pseudo-scaling laws generically decreases with increasing excluded volume fraction, in agreement with several experimental reports. Note finally that these pseudo-scaling regimes usually last less than 1.5 decades and contain 3-5 data points. They are thus very similar to the pseudo-power laws with crowding-dependent exponents that are reported in several experimental as well as numerical studies. Hence these results show that the recurrent experimental reports of crowding-dependent anomalous diffusion exponents could be spurious effects due to a conjugation of finite size effects and poor statistics (w.r.t. simulations).

Even though our results show that the $\left\langle R^2(t)\right\rangle$ vs t relation does not evidence a power law regime (ie a plateau in the $\alpha_{\text{eff}}(t)$ vs t curve), a tentative *approximate* exponent, $\tilde{\alpha}$, during the anomalous regime can be defined in order to, for instance, compare our results with those of works discussing how so-called anomalous scaling exponents vary.

Our objective is to use the minimal value of the $\alpha_{\text{eff}}(t)$ vs t curve. Unfortunately, these curves are usually noisy, with significant "oscillations" superimposed to the overall envelop (see e.g. Figure 1, Bottom row), which precludes naive attempts to use their minimal value as reliable estimates. But these curves (especially their concave part) can nicely be fitted by an inverted Log-Normal function of the form $\alpha_{\text{eff}}(t) = 1 - A\exp\left[-\left(\ln\left(t/t_{min}\right)/w\right)^2\right]$. The estimated value of A then yields the minimum value of the function on the interval, i.e. $\tilde{\alpha} = 1 - A$. $\tilde{\alpha}$ is thus used here as a "rational" estimate of the approximate exponent.

First of all, the measurements of $\tilde{\alpha}$ on our data, in Fig. 2, shows that when plotted against the relative distance to the threshold $\epsilon = 1-\theta/\theta_c$ (θ_c is the value of θ at the percolation threshold), the data for 2d simulations and various molecule sizes collapse on a single behavior. This collapse suggests a generic behavior for approximate exponent that would only depend on space dimension. Moreover, the 2d and 3d data could both be fitted by the same nonlinear function (the lines in Fig. 2):

$$\tilde{\alpha}\left(\epsilon\right) = \tilde{\alpha}_0 + \left(1 - \tilde{\alpha}_0\right)\left(1 + K\right)\frac{\epsilon}{K + \epsilon}. \tag{2}$$

For 2d data, we obtained $K^{(2d)} = 0.75 \pm 0.10$ and $\tilde{\alpha}_0^{(2d)} = 0.69 \pm 0.02$ and $K^{(3d)} = 0.23 \pm 0.03$ and $\tilde{\alpha}_0^{(3d)} = 0.49 \pm 0.01$ for the 3d case. Note that the value of $\tilde{\alpha}$ at the percolation threshold ($\epsilon = 0$) is given by the parameter $\tilde{\alpha}_0$ and is expected to correspond to the theoretical values predicted by percolation theory. In this perspective, our estimates for α_0 are in very good agreement with theoretical values ($\alpha^{(2d)} \approx 0.686$, $\alpha^{(3d)} \approx 0.526$ (2)). Hence, we think that Eq. 2 yields an accurate functional form for the dependence of the approximate anomalous diffusion coefficient on crowding density (see the Discussion section for comparison with experimental results).

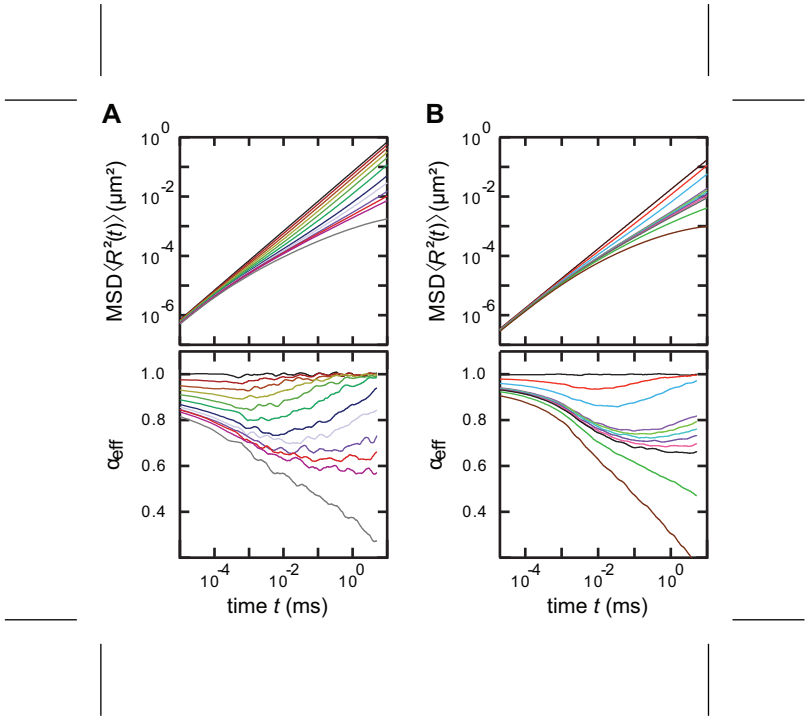

Figure S1: **Evolution of the mean-squared displacement (*Top Row*) and corresponding effective exponent $\alpha_{\rm eff}$ (*Bottom Row*) during hindered diffusion by immobile obstacles in 2D**. (**A**) 2d diffusion of small tracer molecules ($r_{\rm w} = 0.5$ nm, $r_{\rm obs} = 2.0$ nm) with excluded volume fraction $\theta = 0$, 0.10, 0.18, 0.26, 0.33, 0.39, 0.45, 0.48, 0.51, 0.52, 0.53, 0.58 (from top to bottom). Corresponding estimates are $\theta_c = 0.52(2)$ and $\alpha = 0.64(5)$. (**B**) 2d diffusion of point-like tracers ($r_{\rm w} = 0.0$ nm, $r_{\rm obs} = 5.0$ nm) with $\theta = 0$, 0.27, 0.47, 0.61, 0.62, 0.63, 0.648, 0.654, 0.545, 0.72 and 0.79 (from top to bottom); yielding $\theta_c = 0.66(1)$ and $\alpha = 0.69(3)$. All data are averages over 10^4 walkers per obstacle configurations and 10 (A) or 100 (B) obstacle configurations. Other parameters : $D = 4.4$ μm^2/s, $\delta t = 10$ ns (A) or 7.7 μm^2/s and 20 ns, respectively (B), $\delta r = 1.0$ nm and $L_x = L_y = 5.0$ μm .

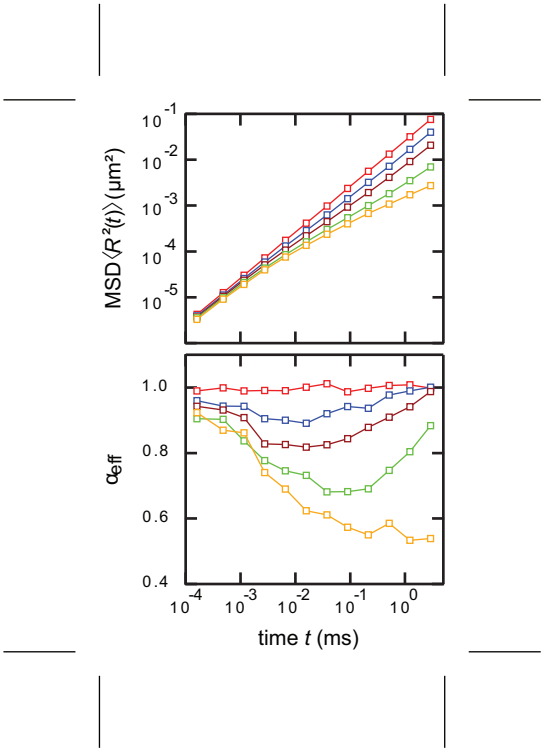

Figure S2: **Simulations of hindered diffusion by immobile obstacles in poor conditions (large finite size effect, low statistics, poor sampling)** . The simulation conditions are identical to figure 1B, i.e. $d = 3$, $r_{\mathrm{w}} = 2.0$ nm, $r_{\mathrm{obs}} = 10.0$ nm except $L_x = L_y = L_z = 0.10$ μm, averaging over 10^3 walkers per obstacle configuration and 3 obstacle configurations and circa 50-fold less data points than in figure 1B (open squares). $\theta = 0$, 0.448, 0.630, 0.773, and 0.851 (from top to bottom). Lines are guides to the eyes.

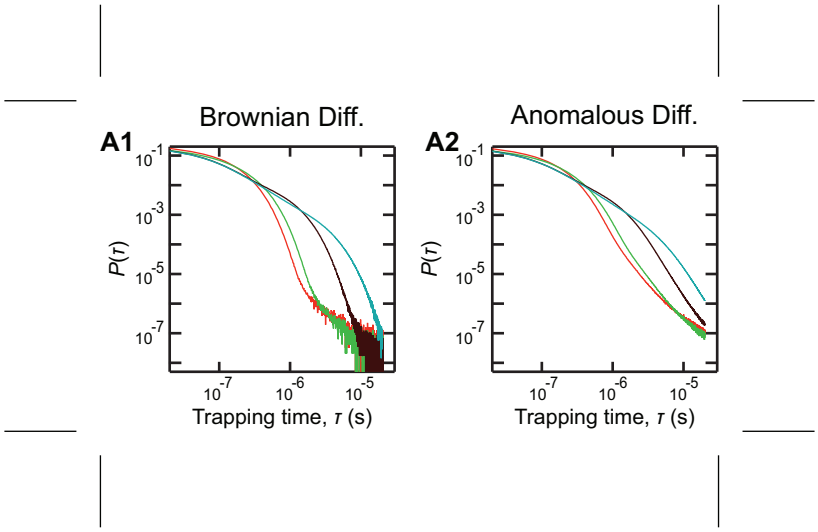

Figure S3: **Trapping times distributions for hindered diffusion by immobile diffusive (B) obstacles**. Same simulation parameters as in Figure 5 except that the obstacles move through Brownian diffusion with diffusion coefficient $D_{\text{obs}}/D = 5.7 \times 10^{-4}$. All other parameters as in Figure 5.